

RESEARCH ARTICLE

10.1002/2013WR015152

Improved flow velocity estimates from moving-boat ADCP measurements

B. Vermeulen¹, M. G. Sassi^{1,2}, and A. J. F. Hoitink¹¹Hydrology and Quantitative Water Management Group, Wageningen University, Wageningen, Netherlands, ²Royal Netherlands Institute for Sea Research, NIOZ, Den Burg, Netherlands

Key Points:

- An improved method to process vessel-mounted ADCP data is introduced
- Standard methods can smooth velocity peaks and miss important flow features
- Few repeat transects are sufficient to filter out effects of turbulence

Correspondence to:

B. Vermeulen,
bart.vermeulen@wur.nl

Citation:

Vermeulen, B., M. G. Sassi, and A. J. F. Hoitink (2014), Improved flow velocity estimates from moving-boat ADCP measurements, *Water Resour. Res.*, 50, doi:10.1002/2013WR015152.

Received 5 DEC 2013

Accepted 1 MAY 2014

Accepted article online 6 MAY 2014

Abstract Acoustic Doppler current profilers (ADCPs) are the current standard for flow measurements in large-scale open water systems. Existing techniques to process vessel-mounted ADCP data assume homogeneous or linearly changing flow between the acoustic beams. This assumption is likely to fail but is nevertheless widely applied. We introduce a new methodology that abandons the standard assumption of uniform flow in the area between the beams and evaluate the drawbacks of the standard approach. The proposed method strongly reduces the extent over which homogeneity is assumed. The method is applied to two field sites: a mildly curved bend near a junction featuring a typical bend flow and a sharply curved bend that features a more complex sheared flow. In both cases, differences are found between the proposed method and the conventional method. The proposed technique yields different results for secondary flow patterns compared with the conventional method. The velocity components estimated with the conventional method can differ over 0.2 m/s in regions of strong shear. We investigate the number of repeat transects necessary to isolate the mean flow velocity vector from the raw ADCP signal, discarding the influences of noise, positioning and projection errors, and turbulence. Results show that several repeat transects are necessary. The minimum number of repeat measurements needed for robust mean velocity estimates is reduced when applying the proposed method.

1. Introduction

Acoustic Doppler current profilers (ADCPs) are the current standard for flow measurements in large-scale open water environments [Dinehart and Burau, 2005b; Buschman et al., 2013; Sassi et al., 2013; Jamieson et al., 2011]. Current techniques to process ADCP data [Kim et al., 2009; Le Bot et al., 2011; Parsons et al., 2013] assume homogeneous flow between the measured radial components of velocity, often referred to as radial velocities (Figure 1a). This homogeneity assumption is often questionable [Marsden and Ingram, 2004], but, nevertheless, widely applied. We propose a technique to process vessel-mounted ADCP data that reduces the volume in which the flow is considered homogeneous. This volume is reduced by abandoning the standard procedure of combining inclined ADCP beams that measure simultaneously. Instead, we combine radial velocities based on their position within a predefined mesh (Figures 1a and 1b). The combination of several radial velocities leads to one, best fitting velocity, estimated with a least squares method. The velocity achieved by this approach can differ up to 40% from that obtained with the conventional approach.

ADCPs do not directly measure the Cartesian components of a velocity vector. The velocity vector can only be reconstructed by combining several radial velocities. This necessarily leads to the common assumption of a homogeneous flow between the measuring locations of the radial velocities. The set of radial velocities that leads to a flow velocity estimate directly determines the extent over which the flow is assumed homogeneous.

At present, vessel-mounted ADCP data processing techniques typically solve for the velocity based on—generally three to four—radial velocity components. These radial velocity measurements originate from the three or four available acoustic beams and are collected during one measuring cycle, and at one specific depth [Marsden and Ingram, 2004; Kawanisi, 2004; Kim et al., 2009; Le Bot et al., 2011; Parsons et al., 2013; Tokyay et al., 2009; Muste et al., 2010; Nystrom et al., 2007; Gargett, 1994]. Since acoustic beams diverge with distance from the ADCP, the distance among the measured radial velocities increases when moving away from the ADCP (Figure 1a). This results in an increase of the volume in which the flow is assumed homogeneous. Although this homogeneity assumption is widely applied, it is likely to fail.

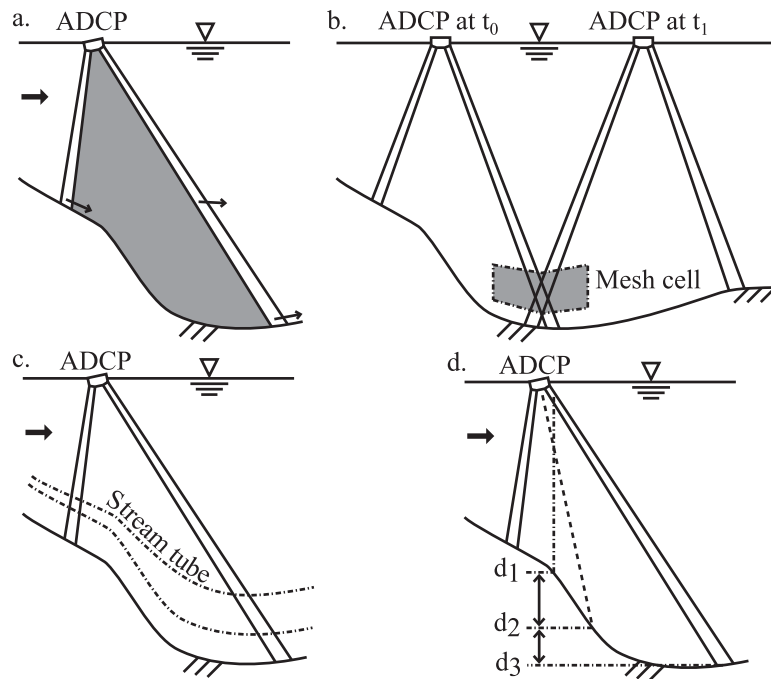


Figure 1. (a) Tilting strongly affects the location where velocity is sampled. The large spread of the beams implies that, when combining velocity samples from different beams directly, the sampling volume is very large (gray area in Figure 1a). This renders the location of the velocity estimate to be unclear. The assumption of flow homogeneity also fails due to the large sampling volume (Figure 1a). A better approach is to combine velocity sampled in the same location (e.g., in a mesh cell indicated as the gray area in Figure 1b) instead of combining velocity sampled simultaneously by the acoustic beams of the ADCP. When bed gradients are present, it is better to combine velocity samples from the same relative depth. Based on a continuity consideration, (c) a stream-tube approach can be adopted. To determine the relative depth, the actual depth of the velocity sample (d_1 in Figure 1d) must be determined. This can differ significantly from the depth at the end of an acoustic beam (d_3) or the average depth of the acoustic beams (d_2).

A way to deal with this inhomogeneity is to apply a correction to account for first-order shearing in the flow [Marsden and Gratton, 1997; Marsden and Ingram, 2004; Kawanisi, 2004]. This correction is achieved by Taylor expansion of the solution of the velocity vector. These corrections were derived for three beams [Kawanisi, 2004] and four beams systems [Marsden and Gratton, 1997; Marsden and Ingram, 2004]. With these corrections, the flow is no longer assumed to be constant but may vary linearly within the measuring volume. The volume in which linear change of the flow is assumed remains, however, unchanged.

There are several conditions that may lead to flow inhomogeneity. Turbulence causes both spatial and temporal variations in the flow. An instantaneous ADCP velocity measurement therefore contains contributions by the mean flow, turbulence, and instrumental noise. Typically, the contribution by turbulence overwhelms the noise effect [Lu and Lueck, 1999; Vermeulen et al., 2011]. Turbulence-induced time variations require vessel-mounted ADCP transects to be navigated repeatedly at the same cross section [Szupiany et al., 2007; Tarrab et al., 2012]. This allows to isolate the mean flow contribution. Turbulence-induced spatial variations affect the quality of velocity estimates by introducing flow inhomogeneity, when the scales involved are smaller than the distance between the acoustic beams [Marsden and Ingram, 2004]. Other sources of inhomogeneity include large gradients in bed topography, mixing layers at confluences, and secondary flows at river bends, which can result in considerable spatial gradients in the mean flow velocity field (Figure 1c).

We introduce a generic approach to estimate flow velocity given an arbitrary set of radial velocities in section 2.1. We explain how to estimate the variance in flow velocity in section 2.2. Subsequently, in section 2.3, we define the mesh in which we estimate velocity. Details about the estimation of ship velocity, defining sections, positioning the velocity data, and nondimensionalizing the depth are given in sections 2.4–2.7. The method is applied to two field cases, yielding results presented in section 3. These results specifically address the homogeneity assumption (section 3.1) and the role of turbulence (section 3.2). We discuss the results and draw conclusions in section 4.

2. Method

2.1. Estimating Velocity

Given an arbitrary set of measured radial velocities, we intend to find a “best fit” mean velocity vector, representing the average over the time span of available transect data. Radial velocities measured within a pre-defined volume contain information about the average velocity of the flow in that volume. The radial velocity measured by an ADCP is the projection of the velocity vector in the direction of the acoustic beam. The direction of the acoustic beam can be described by a unit vector \mathbf{q} . The measured radial velocity b relates to the velocity \mathbf{v} as

$$b = \mathbf{v} \cdot \mathbf{q} = \mathbf{q}^T \mathbf{v}. \quad (1)$$

If we consider a set of N radial velocity samples we can write:

$$\begin{pmatrix} b_1 \\ \vdots \\ b_N \end{pmatrix} = \begin{pmatrix} \mathbf{q}_1^T \\ \vdots \\ \mathbf{q}_N^T \end{pmatrix} \mathbf{v} \iff \mathbf{b} = \mathbf{Q}\mathbf{v}, \quad (2)$$

where \mathbf{v} may be replaced with a Taylor expansion around the center of the volume spanned by a set of radial velocities [Marsden and Ingram, 2004; Kawanisi, 2004] to account for remaining inhomogeneities. In practice, the radial velocity will be affected by instrument noise, the effect of turbulence, spatial inhomogeneity, and other errors:

$$\mathbf{b} = \mathbf{Q}\mathbf{v} + \epsilon, \quad (3)$$

in which ϵ is the combined effect of all errors. The solution for the velocity is found in such a way that the sum of squared errors $\hat{\epsilon}^T \hat{\epsilon}$ is minimized. The estimate of the velocity \mathbf{v} reads [Johnson and Wichern, 2007; Vermeulen et al., 2011]:

$$\hat{\mathbf{v}} = \mathbf{Q}^+ \mathbf{b}, \quad (4)$$

in which $\mathbf{Q}^+ = (\mathbf{Q}^T \mathbf{Q})^{-1} \mathbf{Q}^T$ is the generalized inverse of \mathbf{Q} . The matrix \mathbf{Q} can be rank deficient when the number of radial velocity estimates included is too small. A single repeat transect already yields sufficient samples to invert \mathbf{Q} , provided the vessel speed is not too high.

2.2. Estimating Velocity Variance

The residuals ϵ can be estimated as

$$\hat{\epsilon} = \mathbf{b} - \mathbf{Q}\hat{\mathbf{v}}. \quad (5)$$

From this, we can also obtain the covariance matrix of the velocity estimator [Johnson and Wichern, 2007]

$$\text{var}(\hat{\mathbf{v}}) = \frac{\hat{\epsilon}^T \hat{\epsilon} (\mathbf{Q}^T \mathbf{Q})^{-1}}{N-3}. \quad (6)$$

This relates to the velocity covariance as in

$$\text{var}(\hat{\mathbf{v}}) = \frac{\text{var}(\mathbf{v})}{N}. \quad (7)$$

The estimate of residuals in radial velocity can be used to remove possible outliers.

2.3. Meshing

The navigated section during a repeat transect can be subdivided in small volumes by defining a mesh. All radial velocities within a mesh cell, from several repeat transects, are used to solve for the flow velocity according to section 2.1.

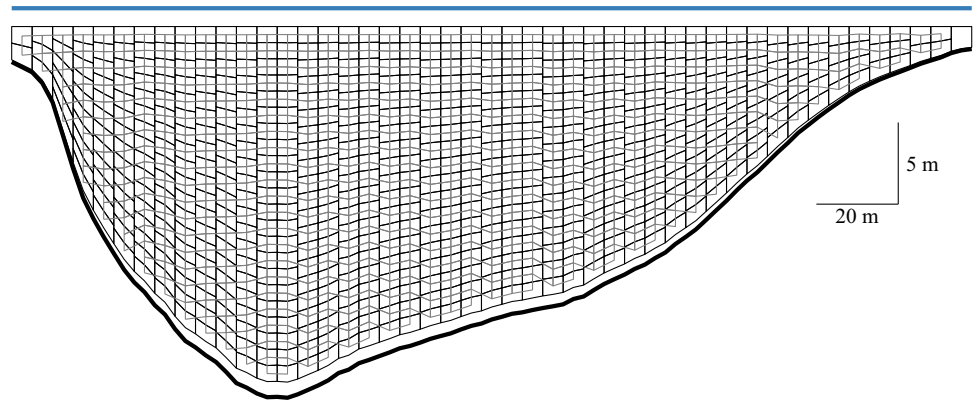


Figure 2. Example of a mesh generated for velocity processing at section 8 (Figure 4). The mesh follows in each vertical the bed in the same way a sigma-mesh would do, but has a varying number of cells in the vertical, to ensure a nearly equal number of velocity samples in each mesh cell. The gray lines indicate the connectivity between the cells, necessary for the computation of derivatives.

The mesh generation procedure starts by subdividing the section in vertical slices with a user-defined width (Δn). The lower boundary of the mesh is set to the lowest part of the water column not influenced by side-lobes (in our case 0.06 of the water depth). The upper boundary is determined by the highest location where a radial velocity sample is available.

Subsequently, each of the vertical slices is split in several cells. The available vertical distance is subdivided in an integral number of parts such that the given vertical mesh size (Δz) is best resembled. A mesh cell will have six edges, two on the left side, two in the middle, and two on the right side (see mesh in Figure 2). Eventually, the vertical z coordinates of the mesh are converted to nondimensional coordinates σ , as defined in equation (11). The mesh itself defines an intrinsic coordinate system (v, ζ) , corresponding to rows and columns. The connectivity of neighboring cells is chosen such that the vertical coordinate z remains relatively constant for a constant value of ζ (Figure 2). Since this is not everywhere the case, we need to apply a correction to the computation of the derivatives. The gradient of a quantity defined on the mesh can be computed as

$$\begin{pmatrix} \frac{\partial}{\partial n} \\ \frac{\partial}{\partial z} \end{pmatrix} = \begin{pmatrix} \frac{\partial v}{\partial n} & \frac{\partial \zeta}{\partial n} \\ \frac{\partial v}{\partial z} & \frac{\partial \zeta}{\partial z} \end{pmatrix} \begin{pmatrix} \frac{\partial}{\partial v} \\ \frac{\partial}{\partial \zeta} \end{pmatrix}, \quad (8)$$

where n is the horizontal coordinate on the section plane. All derivatives are approximated based on centered differences.

2.4. Estimating Ship Velocity

The raw radial velocity samples have to be corrected for the ship velocity. One way to estimate ship velocity is to use a so-called bottom-ping, which estimates the vessel speed with respect to the river bed, assumed to be fixed. This method fails when the range to the bed is too high, or when the river bed is moving due to bed-load sediment transport [Rennie *et al.*, 2002; Sassi *et al.*, 2011]. An alternative method requires the use of an accurate GPS to estimate ship velocity. In this study, all raw radial velocities were corrected for the ship velocity, transformed to radial components, based on DGPS data. The use of GPS as a reference is not a pre requisite for the application of the proposed method.

2.5. Transect Splitting and Section Definition

The track navigated by the vessel during data collection is defined by all positions of the ADCP, \mathbf{p}_a , expressed in a projected geographic coordinate system (x, y, z) , and usually collected with a GPS device (the vertical component z of \mathbf{p}_a is set to the draft of the ADCP transducers). The track is split into single crossings, each belonging to a river section (Figures 3 and 4), based on which the data will be further processed. For each section, we define a direction, which together with the vertical (\mathbf{k}), defines a plane on which the data will be projected. The direction of a section \mathbf{t} is determined as the largest eigenvector of the covariance matrix of \mathbf{p}_a . The horizontal direction, orthogonal to \mathbf{t} , is defined by the unit vector \mathbf{o} (Figures 3 and 4). Any position \mathbf{p} is transformed to a coordinate system defined on the section plane

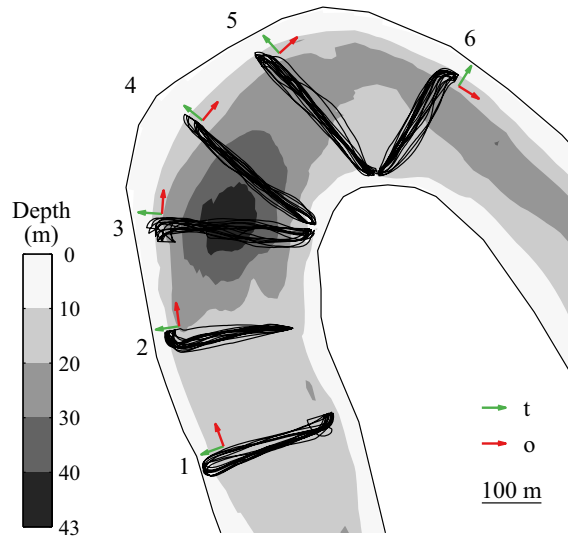


Figure 3. Track navigated by the vessel, included in the data processing at a sharp bend exemplifying the new method. The flow in the figure is in the direction of the \mathbf{o} vectors. The track is divided in several sections indicated by a number. For each section, the along section direction \mathbf{t} and orthogonal direction \mathbf{o} are indicated by the arrows in the colors green and red, respectively.

of \mathbf{T} will mainly depend on the way the instrument measures the three consecutive rotations. The position of a radial velocity measurement at a range r from the instrument is

$$\mathbf{p} = \mathbf{p}_a + r\mathbf{q}. \quad (10)$$

The same approach is followed to determine the position of the bed based on the range to the bed measured by the ADCP.

2.7. Nondimensional Depth

Commonly, when processing ADCP data, the depth detected at the end of the beam is considered representative for all measurements performed along that beam. This can be correct when the gradient in the bed elevation is limited. When strong bed level gradients are present, the depth at a velocity measurement can be quite different from the depth at the end of the acoustic beam (see Figure 1d). The proper depth at

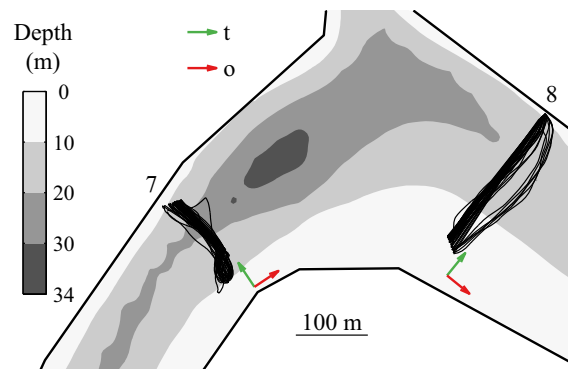


Figure 4. The track navigated by the vessel is divided in two sections indicated by numbers. The flow in the main channel at the bottom of the figure is in the direction of the \mathbf{o} vectors. The flow in the side-channel at the top is from top to bottom. For each vector, the along section direction \mathbf{t} and the orthogonal direction \mathbf{o} are indicated by the arrows in the colors green and red, respectively.

$$\begin{pmatrix} s \\ n \\ z \end{pmatrix} = \begin{pmatrix} (\mathbf{p} - \overline{\mathbf{p}}_a) \cdot \mathbf{o} \\ (\mathbf{p} - \overline{\mathbf{p}}_a) \cdot \mathbf{t} \\ \mathbf{p} \cdot \mathbf{k} \end{pmatrix}, \quad (9)$$

where $\overline{\mathbf{p}}_a$ denotes the average of all track positions belonging to a certain section.

2.6. Positioning of Radial Velocities

The location of the radial velocity sample determines which mesh cell the radial velocities belong to. In an ADCP-centered coordinate system, the spatial orientation of the acoustic beams of an ADCP can be described by a unit vectors $\hat{\mathbf{q}}$ for each beam. To account for the orientation of the ADCP during data collection, we need to rotate the coordinate system to the projected geographic coordinate system $\mathbf{q} = \mathbf{T}\hat{\mathbf{q}}$. The rotation matrix \mathbf{T} is usually composed of three consecutive rotations in space that transform the ADCP-fitted coordinate system to a projected geographic coordinate system. The definition

of \mathbf{T} will mainly depend on the way the instrument measures the three consecutive rotations. The position

at each radial velocity is found by interpolation from a predetermined bathymetry. This bathymetry is constructed using all depth measurements obtained with the ADCP. For each velocity measurement position, \mathbf{p}_v , we therefore find the corresponding bed position \mathbf{p}_b . With the obtained bed position, we nondimensionalize the vertical coordinate:

$$\begin{pmatrix} s \\ n \\ \sigma \end{pmatrix} = \begin{pmatrix} (\mathbf{p}_v - \overline{\mathbf{p}}_a) \cdot \mathbf{o} \\ (\mathbf{p}_v - \overline{\mathbf{p}}_a) \cdot \mathbf{t} \\ 1 - \frac{\mathbf{p}_v \cdot \mathbf{k} - \eta}{\mathbf{p}_b \cdot \mathbf{k} - \eta} \end{pmatrix}, \quad (11)$$

where η is the fluctuation of water level around the mean water level at which $z = 0$.

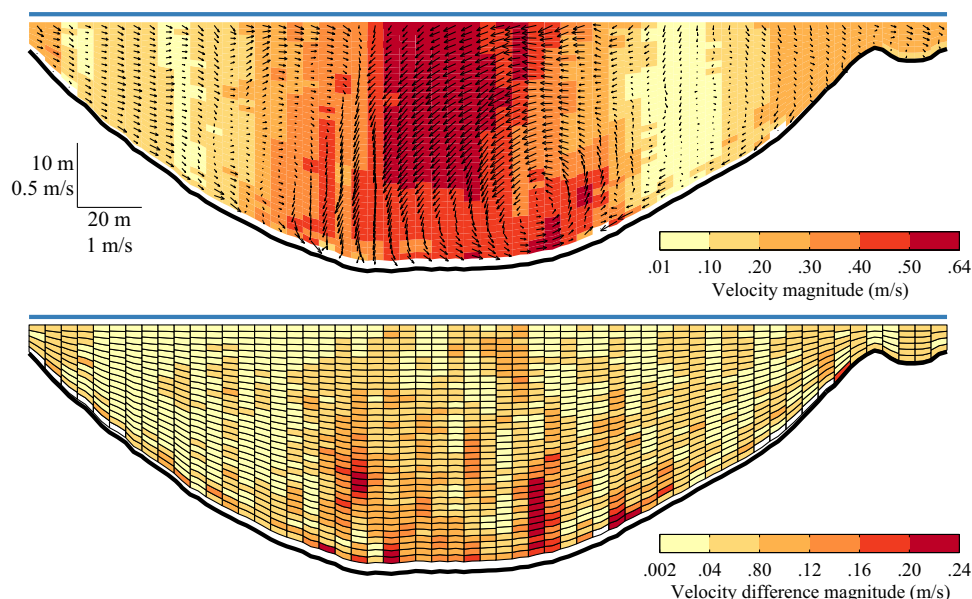


Figure 5. (top) The flow pattern at section 3 (Figure 3) based on the proposed method. The colors indicate the longitudinal velocity component, while the arrows indicate the velocity components in the section plane. In horizontal direction, there is a strong shearing in the flow. This results in large differences between the conventional processing method and the method proposed.

3. Results

We process two data sets according to the proposed method. The data were collected at two locations along the Mahakam River, East Kalimantan, Indonesia. This river features several bends with very deep scour holes often exceeding three times the average depth, reaching depths of typically 45 m [B. Vermeulen et al., Sharp bends associated with deep scours in a tropical river: The River Mahakam, submitted to *Journal of Geophysical Research: Earth Surf*, 2013]. We selected two locations, one featuring a strongly sheared flow near a sharp bend (Figure 3) and another at a mild bend near a junction (Figure 4).

The two data sets are processed both according to the proposed method and according to the conventional processing approach. The conventional method differs from the proposed method only in the way velocity vectors are estimated, i.e., directly from simultaneously measured radial velocities, from each of the four ADCP beams.

3.1. Flow Inhomogeneity

At large distance from the ADCP, differences between the two methods are most pronounced, because the beam spreading increases with depth from the surface. The difference between the two methods reaches in some areas values of 0.24 m/s, which is a significant portion of the total magnitude of the estimated velocity (Figure 5). These large differences not only occur in sections with complex flows. Also at section 7, with a relatively simple flow pattern including a secondary circulation cell due to curving of the river, differences are high compared to the total magnitude of the velocity (Figure 6). The vertical component in the uppermost velocity estimates appears to be biased low. This can be attributed to the effect of the vessel interfering with the flow [Tokay et al., 2009; Muste et al., 2010; Jamieson et al., 2011].

Thirty percent of the cells have a relative difference in longitudinal velocity between 0 and -10% (Figure 7). The difference in longitudinal velocity between the two methods can exceed 20 cm/s. When integrated over the cross section, differences become insignificant. This shows that the conventional method acts as an effective smoother, such that variance is reduced, but the longitudinal flow is preserved.

Velocity estimates differ most in the cross-stream and vertical direction (Figures 7b and 7c). Only about 15% of the cells have a relative difference in velocity magnitude of less than 10%. The remainder of the cross

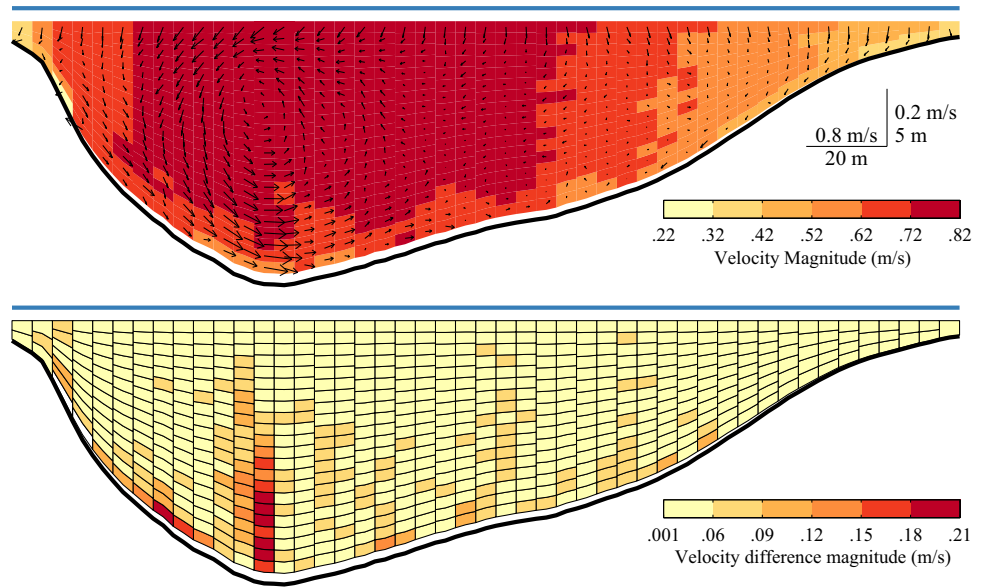


Figure 6. (top) Secondary flow at section 8 (Figure 4) based on the proposed method. The flow is typical for a mildly curved bend. The magnitude of velocity differences between results from the proposed and the conventional methods shows large differences where (bottom) the flow is inhomogeneous over the area between the acoustic beams.

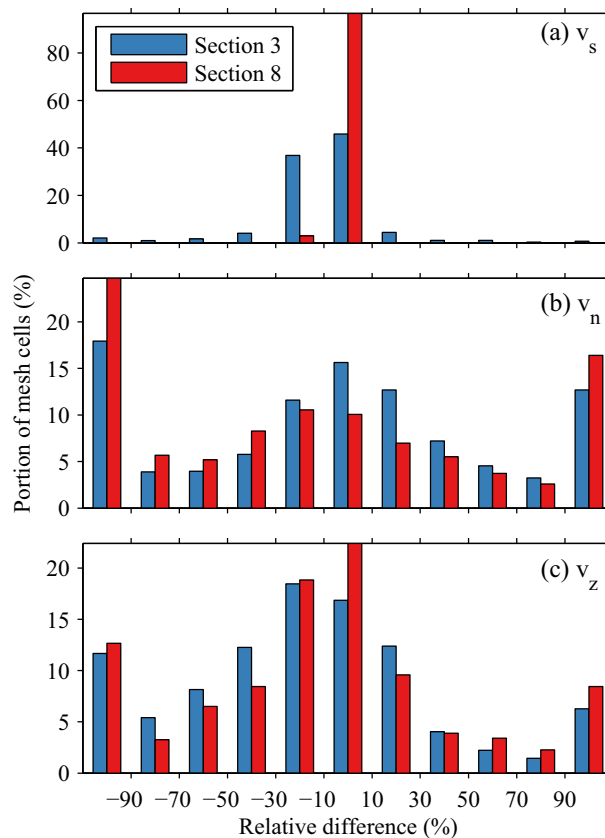


Figure 7. Histograms of relative error in the (a) streamwise, (b) cross-stream, and (c) vertical velocity components at section 3 and section 8. A positive error indicates an overestimation based on the conventional method.

sections show higher differences. The new method results in secondary flow velocity estimates which are markedly different from those obtained with the conventional method. The large number of samples with differences exceeding 100% is mainly resulting from low values of secondary velocity.

The streamwise vorticity of the flow (Figure 8) seems smoother in the conventional method compared to the proposed method. The reason for this can be the fact that the conventional method combines velocity samples collected at much larger distances than the proposed method, introducing spatial smoothing. The secondary flow patterns are different between the two methods. A secondary flow cell clearly visible in the results obtained with the proposed technique is resolved differently in the results obtained with the conventional method (Figure 8). The core of the secondary flow cell is located closer to the bed in the conventional method and below the core no flow toward the inner bank (to the right in Figure 8) is observed. The largest differences in secondary flow occur at locations with strong shearing.

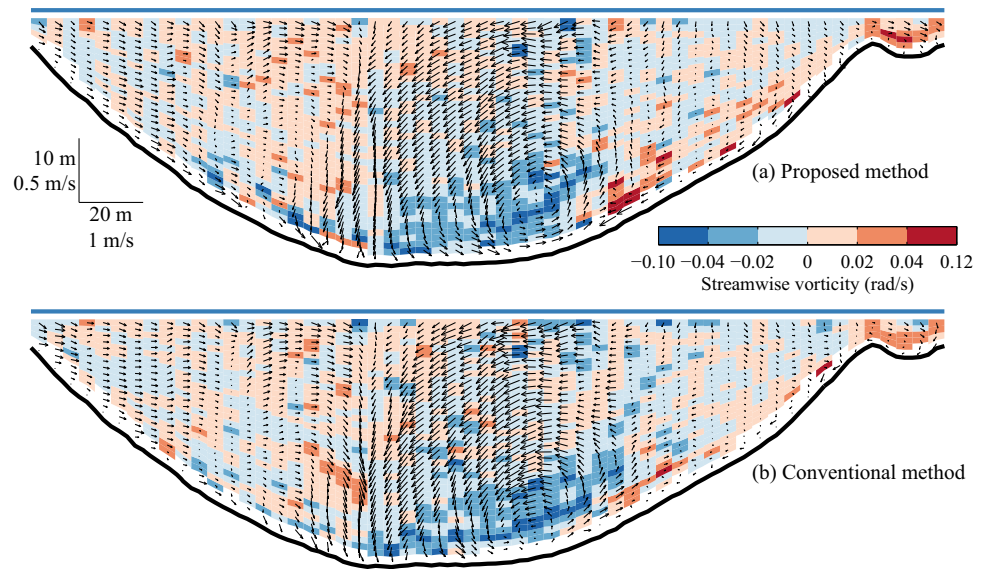


Figure 8. Streamwise vorticity for section 3, determined (a) with the proposed method and (b) with the conventional method.

3.2. Turbulence and Inhomogeneity

The estimated variances (equations (6) and (7)) of the velocity are strongly influenced by the flow inhomogeneity within a mesh cell. The estimated variance for the conventional method is determined as the variance of the Cartesian estimators of velocity within a mesh cell. We can expect this variance to be biased low, compared to the variance estimated for the proposed method, since we do not take into account the variance in the initial radial velocities.

When more repeat transects are included in the estimate of the velocity variance, we expect the variance to increase until enough repeat transects are included. The variance will only reach a stable value under steady flow conditions [Soulsby, 1980]. Once a stable value of the variance estimate is obtained, it is reasonable to conclude that enough data were collected to obtain a robust estimate of the mean velocity vector. This analysis was performed with different cell sizes (Figure 9).

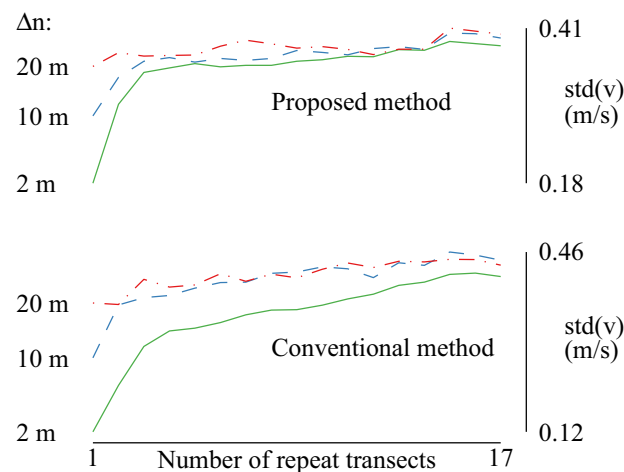


Figure 9. Standard deviation of the velocity estimated at section 3. The top graph is based on results from the proposed method. The lower graph is based on results from the conventional method. River crossings were progressively included to estimate the standard deviation in velocity, for different horizontal mesh cell sizes.

For section 3, the variance is increasing when more repeat transects are included. This is attributed to a higher temporal coverage of turbulence-induced fluctuations. At a certain number of repeat transects, the estimated variances in velocity stabilize. Typically, four to five repeat transects are needed when using the proposed method, while many more transects are needed when the conventional method is adopted. The improvement in variance convergence is most pronounced for smaller mesh cell sizes. This can be explained by the fact that the current method provides the largest improvements when the cell size is much smaller than the beam spread.

The estimates of variance, which is mostly caused by turbulence, benefit more from the inclusion of additional repeat transects than from a larger mesh

cell size. These results confirm earlier findings by *Tarrab et al.* [2012]. Increasing the mesh cell size, or applying a spatial smoother, only improves the estimates of the spatially induced variance. The temporal component of the variance is strongly improved when including more repeat transects. Due to ship motions, this variance cannot be used to estimate turbulence properties [*Lu and Lueck*, 1999].

4. Discussion and Conclusions

A new method is proposed to yield improved velocity estimates from moving-boat measurements. The new method abandons direct combination of velocity estimates from the four acoustic beams to a Cartesian velocity vector, which is intuitively appealing, and has gained wide acceptance. Since the acoustic beams are divergent and sample synchronously, velocity estimates from three beams at the same horizontal level yield the instantaneous Cartesian velocity vector, provided that the instantaneous velocity field between the three beams at that level is spatially homogeneous. The latter assumption is largely valid for the mean flow but not for turbulence-induced velocity fluctuations [*Vermeulen et al.*, 2011; *Stacey et al.*, 1999]. To some degree, the fourth acoustic beam can be used to reduce the effect of spatial inhomogeneity of turbulent fluctuations, but repeat transects are indispensable to remove it completely, and to take out the effect of temporal variation. In the new method, the mean Cartesian velocity vector is retrieved in a single step based on a least squares procedure.

The proposed method reduces the spatial extent of the region over which turbulence-averaged properties are assumed to be homogeneous, which applies both to the conventional and to the proposed method. In the conventional approach, the quality of the velocity estimates generally deteriorates with distance from the transducer, because of the increasing aperture between the beams. Also, instrument tilts directly lead to a loss of accuracy, depending on the distance to the transducer. The new approach features a very generic way of dealing with beam spreading and instrument tilts and can be applied to any beam configuration. It can also be extended to perform a first-order correction for the inhomogeneity [*Marsden and Ingram*, 2004; *Kawanisi*, 2004].

The method is shown to provide results that differ from results obtained with conventional processing methods. The method allows to better recognize secondary flow cells. Beam divergence acts as a spatial filter [*González-Castro and Muste*, 2007], with a filtering window that increases with distance from the ADCP transducer. This leads to a reduction of the variance in velocities but leaves the cross-section integrated velocity unaffected.

Our results confirm earlier findings of *Szupiany et al.* [2007] and *Tarrab et al.* [2012], who argue that several repeat transects are needed to obtain robust estimates of the turbulence-averaged velocity. The proposed method seems to reduce the minimum number of repeat transects needed. When estimating the variance in velocity, progressively including more repeat transects is shown to be an effective method to assess the effect of turbulence-induced inhomogeneities on the estimated velocity. A single repeat transect already yields sufficient data to estimate the velocity vector, which holds both for the proposed method and for the conventional method. The inclusion of a larger number of repeat transects serves to isolate the mean velocity vector but is not a prerequisite to apply the proposed method. Mean velocity estimates obtained either from the conventional method or from the new method suffer from errors in positioning and projection, essentially in the same way. The solution to the problem of beam divergence presented here comes at no extra cost other than restrictions to the mesh, to guarantee enough velocity samples in each mesh cell.

The new method can have far-reaching implications for those using vessel-mounted ADCPs for flow velocity measurements. The relevance for procedures to obtain river discharge [e.g., *Gordon*, 1989; *Le Coz et al.*, 2008; *Nihei and Kimizu*, 2008; *Sassi et al.*, 2011; *Hidayat et al.*, 2011] is limited, since cross-section averaged velocity is largely unaffected. Secondary flow patterns appear to be different with the proposed method, resulting in different positioning of the core of secondary recirculations. It will be particularly relevant for studies of complex geophysical surface flows, focusing on sediment transport [e.g., *Rennie et al.*, 2002; *Thorne and Hanes*, 2002; *Hoitink*, 2004; *Hoitink and Hoekstra*, 2005; *Kostaschuk et al.*, 2005; *Parsons et al.*, 2005; *Buschman et al.*, 2012; *Moore et al.*, 2012; *Sassi et al.*, 2012; *Szupiany et al.*, 2012], flow division at bifurcations [e.g., *Richardson and Thorne*, 2001; *Dinehart and Burau*, 2005a; *Sassi et al.*, 2012; *Buschman et al.*, 2013] or detailed flow patterns related to channel junctions [e.g., *Rhoads and Sukhodolov*, 2001; *Dinehart and Burau*, 2005a; *Lane et al.*, 2008], and near obstacles [e.g., *Jamieson et al.*, 2011; *Le Coz et al.*, 2010].

5. Software Availability

The methods presented have been implemented in a set of open-source MATLAB functions. They have been made available at <http://adcptools.googlecode.com>. Processing is performed combining binary input files and NMEA-based ASCII input files.

Notation

x	eastward coordinate (along \hat{i}).
y	northward coordinate (along \hat{j}).
z	upward coordinate (along \hat{k}).
n	along section coordinate (along \hat{t}).
s	across section coordinate (along \hat{o}).
Δn	lateral mesh size.
Δz	vertical mesh size.
v	intrinsic horizontal mesh coordinate (along rows).
ζ	intrinsic vertical mesh coordinate (along columns).
σ	nondimensional elevation above the bed (along \hat{k}).
b	radial beam component of velocity (along \hat{q}).
N	number of velocity samples collected in a mesh cell.
\hat{i}	east pointing unit vector.
\hat{j}	north pointing unit vector.
\hat{k}	upward pointing unit vector.
\hat{t}	along section pointing unit vector.
\hat{o}	across section pointing unit vector.
\hat{q}	unit vector pointing in direction of an acoustic beam, toward the instrument.
\mathbf{p}	vector indicating position.
\mathbf{p}_a	vector indicating ADCP position.
$\bar{\mathbf{p}}_a$	average of all ADCP positions belonging to a section.
\mathbf{p}_b	vector indicating bed position.
\mathbf{v}	velocity.
ϵ	velocity model errors.
\mathbf{Q}	matrix to change from radial beam coordinate system to geographic coordinate system. It is a collection of several \hat{q}^T .
\mathbf{T}	Rotation matrix to transform an instrument centered Cartesian coordinate system to a geographic coordinate system.
\sim	accent denoting instrument coordinate system.
$\hat{}$	accent denoting an estimator.
T	transposed of a matrix.
$^{-1}$	inverse of a matrix.
$+$	generalized inverse of a matrix.

Acknowledgments

This research has been supported by the Netherlands organization for scientific research (NWO grant number WT76–268). The authors would like to thank David Vermaas and Frans Buschman for contributing to the development and testing of the ADCP processing tools. Thanks to Hidayat, Fajar Setiawan, Unggul Handoko, Ulfah Karmilasari, and Supriadi for their help during the data collection. Wawan Kustiawan and Y. Budi Sulistioadi (Mulawarman University) are thanked for facilitating the fieldwork. We thank Pieter Hazenberg and Johan Romeligh for the technical support. The authors thank two anonymous reviewers and the associate editor for their constructive comments that helped improving the manuscript.

References

- Buschman, F. A., A. J. F. Hoitink, S. M. de Jong, P. Hoekstra, H. Hidayat, and M. G. Sassi (2012), Suspended sediment load in the tidal zone of an Indonesian river, *Hydrol. Earth Syst. Sci.*, *16*(11), 4191–4204, doi:10.5194/hess-16-4191-2012.
- Buschman, F. A., M. van der Vegt, A. J. F. Hoitink, and P. Hoekstra (2013), Water and suspended sediment division at a stratified tidal junction, *J. Geophys. Res.: Oceans*, *118*, 1459–1472, doi:10.1002/jgrc.20124.
- Dinehart, R., and J. Burau (2005a), Repeated surveys by acoustic Doppler current profiler for flow and sediment dynamics in a tidal river, *J. Hydrol.*, *314*(1–4), 1–21, doi:10.1016/j.jhydrol.2005.03.019.
- Dinehart, R. L., and J. R. Burau (2005b), Averaged indicators of secondary flow in repeated acoustic Doppler current profiler crossings of bends, *Water Resour. Res.*, *41*, W09405, doi:10.1029/2005WR004050.
- Gargett, A. E. (1994), Observing turbulence with a modified acoustic Doppler current profiler, *J. Atmos. Oceanic Technol.*, *11*(6), 1592–1610, doi:10.1175/1520-0426(1994)011<1592:OTWAMA>2.0.CO;2.
- González-Castro, J., and M. Muste (2007), Framework for estimating uncertainty of ADCP measurements from a moving boat by standardized uncertainty analysis, *J. Hydraul. Eng.*, *133*(12), 1390–1410, doi:10.1061/(ASCE)0733-9429(2007)133:12(1390).
- Gordon, R. (1989), Acoustic measurement of river discharge, *J. Hydraul. Eng.*, *115*(7), 925–936, doi:10.1061/(ASCE)0733-9429(1989)115:7(925).
- Hidayat, H., B. Vermeulen, M. G. Sassi, P. J. J. F. Torfs, and A. J. F. Hoitink (2011), Discharge estimation in a backwater affected meandering river, *Hydrol. Earth Syst. Sci.*, *15*(8), 2717–2728, doi:10.5194/hess-15-2717-2011.

- Hoitink, A. (2004), Tidally-induced clouds of suspended sediment connected to shallow-water coral reefs, *Marine Geol.*, 208(1), 13–31, doi:10.1016/j.margeo.2004.04.021.
- Hoitink, A., and P. Hoekstra (2005), Observations of suspended sediment from ADCP and OBS measurements in a mud-dominated environment, *Coastal Eng.*, 52(2), 103–118, doi:10.1016/j.coastaleng.2004.09.005.
- Jamieson, E. C., C. D. Rennie, R. B. Jacobson, and R. D. Townsend (2011), 3-D flow and scour near a submerged wing dike: ADCP measurements on the Missouri River, *Water Resour. Res.*, 47, W07544, doi:10.1029/2010WR010043.
- Johnson, R. A., and D. W. Wichern (2007), *Applied Multivariate Statistical Analysis*, 773 pp., Pearson Prentice Hall, Upper Saddle River, N. J.
- Kawanisi, K. (2004), Structure of turbulent flow in a shallow tidal estuary, *J. Hydraul. Eng.*, 130(4), 360–370, doi:10.1061/(ASCE)0733-9429(2004)130:4(360).
- Kim, D., M. Muste, D. S. Mueller, and M. Winkler (2009), A quick tutorial for using VMS. Coastal and Hydraulics Laboratory - Engineer Research and Development Center - US Army Corps of Engineers. [Available at http://chl.erdc.usace.army.mil/Media/11/12/0/VMS_quick_tutorial.pdf].
- Kostaschuk, R., J. Best, P. Villard, J. Peakall, and M. Franklin (2005), Measuring flow velocity and sediment transport with an acoustic Doppler current profiler, *Geomorphology*, 68(1–2), 25–37, doi:10.1016/j.geomorph.2004.07.012.
- Lane, S. N., D. R. Parsons, J. L. Best, O. Orfeo, R. A. Kostaschuk, and R. J. Hardy (2008), Causes of rapid mixing at a junction of two large rivers: Río Paraná and Río Paraguay, Argentina, *J. Geophys. Res.*, 113, F02024, doi:10.1029/2006JF000745.
- Le Bot, P., C. Kermabon, P. Lherminier, and F. Gaillard (2011), CASCADE V6.1: Logiciel de validation et de visualisation des mesures ADCP de coque, *Tech. Rep. OPS/LPO 11-01*, Ifremer, Centre de Brest, France.
- Le Coz, J., G. Pierrefeu, and A. Paquier (2008), Evaluation of river discharges monitored by a fixed side-looking Doppler profiler, *Water Resour. Res.*, 44, W00D09, doi:10.1029/2008WR006967.
- Le Coz, J., M. Michalková, A. Hauet, M. Comaj, G. Dramais, K. Holubová, H. Piégay, and A. Paquier (2010), Morphodynamics of the exit of a cutoff meander: Experimental findings from field and laboratory studies, *Earth Surf. Processes Landforms*, 35(3), 249–261, doi:10.1002/esp.1896.
- Lu, Y., and R. G. Lueck (1999), Using a broadband ADCP in a tidal channel. Part II: Turbulence, *J. Atmos. Oceanic Technol.*, 16(11), 1568–1579, doi:10.1175/1520-0426(1999)016<1568:UABAA>2.0.CO;2.
- Marsden, R. F., and Y. Gratton (1997), A method for correcting vertical velocities measured from a vessel-mounted acoustic Doppler current profiler, *J. Atmos. Oceanic Technol.*, 14(6), 1533–1538, doi:10.1175/1520-0426(1997)014<1533:AMFCVV>2.0.CO;2.
- Marsden, R. F., and R. G. Ingram (2004), Correcting for beam spread in acoustic Doppler current profiler measurements, *J. Atmos. Oceanic Technol.*, 21(9), 1491–1498, doi:10.1175/1520-0426(2004)021<1491:CFBSIA>2.0.CO;2.
- Moore, S., J. L. Coz, D. Hurther, and A. Paquier (2012), On the application of horizontal ADCPs to suspended sediment transport surveys in rivers, *Cont. Shelf Res.*, 46(0), 50–63, doi:10.1016/j.csr.2011.10.013.
- Muste, M., D. Kim, and J. Gonzalez-Castro (2010), Near-transducer errors in ADCP measurements: Experimental findings, *J. Hydraul. Eng.*, 136(5), 275–289, doi:10.1061/(ASCE)HY.1943-7900.0000173.
- Nihei, Y., and A. Kimizu (2008), A new monitoring system for river discharge with horizontal acoustic Doppler current profiler measurements and river flow simulation, *Water Resour. Res.*, 44, W00D20, doi:10.1029/2008WR006970.
- Nystrom, E. A., C. R. Rehmann, and K. A. Oberg (2007), Evaluation of mean velocity and turbulence measurements with ADCPs, *J. Hydraul. Eng.*, 133(12), 1310–1318, doi:10.1061/(ASCE)0733-9429(2007)133:12(1310).
- Parsons, D. R., J. L. Best, O. Orfeo, R. J. Hardy, R. Kostaschuk, and S. N. Lane (2005), Morphology and flow fields of three-dimensional dunes, Río Paraná, Argentina: Results from simultaneous multibeam echo sounding and acoustic Doppler current profiling, *J. Geophys. Res.*, 110, F04S03, doi:10.1029/2004JF000231.
- Parsons, D. R., P. R. Jackson, J. A. Czuba, F. L. Engel, B. L. Rhoads, K. A. Oberg, J. L. Best, D. S. Mueller, K. K. Johnson, and J. D. Riley (2013), Velocity mapping toolbox (VMT): A processing and visualization suite for moving-vessel ADCP measurements, *Earth Surf. Processes Landforms*, 38, 1244–1260, doi:10.1002/esp.3367.
- Rennie, C., R. Millar, and M. Church (2002), Measurement of bed load velocity using an acoustic Doppler current profiler, *J. Hydraul. Eng.*, 128(5), 473–483, doi:10.1061/(ASCE)0733-9429(2002)128:5(473).
- Rhoads, B. L., and A. N. Sukhodolov (2001), Field investigation of three-dimensional flow structure at stream confluences: 1. Thermal mixing and time-averaged velocities, *Water Resour. Res.*, 37(9), 2393–2410, doi:10.1029/2001WR000316.
- Richardson, W., and C. R. Thorne (2001), Multiple thread flow and channel bifurcation in a braided river: Brahmaputra–Jamuna River, Bangladesh, *Geomorphology*, 38(3–4), 185–196, doi:10.1016/S0169-555X(00)00080-5.
- Sassi, M. G., A. J. F. Hoitink, B. Vermeulen, and Hidayat (2011), Discharge estimation from H-ADCP measurements in a tidal river subject to sidewall effects and a mobile bed, *Water Resour. Res.*, 47, W06504, doi:10.1029/2010WR009972.
- Sassi, M. G., A. J. F. Hoitink, and B. Vermeulen (2012), Impact of sound attenuation by suspended sediment on ADCP backscatter calibrations, *Water Resour. Res.*, 48, W09520, doi:10.1029/2012WR012008.
- Sassi, M. G., A. J. F. Hoitink, B. Vermeulen, and H. Hidayat (2013), Sediment discharge division at two tidally influenced river bifurcations, *Water Resour. Res.*, 49, 2119–2134, doi:10.1002/wrcr.20216.
- Soulsby, R. L. (1980), Selecting record length and digitization rate for near-bed turbulence measurements, *J. Phys. Oceanogr.*, 10(2), 208–219, doi:10.1175/1520-0485(1980)010<0208:SRLADR>2.0.CO;2.
- Stacey, M. T., S. G. Monismith, and J. R. Burau (1999), Measurements of Reynolds stress profiles in unstratified tidal flow, *J. Geophys. Res.*, 104(C5), 10,933–10,949, doi:10.1029/1998JC900095.
- Szupiany, R., M. Amsler, J. Best, and D. Parsons (2007), Comparison of fixed- and moving-vessel flow measurements with an aDp in a large river, *J. Hydraul. Eng.*, 133(12), 1299–1309, doi:10.1061/(ASCE)0733-9429(2007)133:12(1299).
- Szupiany, R. N., M. L. Amsler, J. Hernandez, D. R. Parsons, J. L. Best, E. Fornari, and A. Trento (2012), Flow fields, bed shear stresses, and suspended bed sediment dynamics in bifurcations of a large river, *Water Resour. Res.*, 48, W11515, doi:10.1029/2011WR011677.
- Tarrab, L., C. M. Garca, M. I. Cantero, and K. Oberg (2012), Role of turbulence fluctuations on uncertainties of acoustic Doppler current profiler discharge measurements, *Water Resour. Res.*, 48, W06507, doi:10.1029/2011WR011185.
- Thorne, P. D., and D. M. Hanes (2002), A review of acoustic measurement of small-scale sediment processes, *Cont. Shelf Res.*, 22(4), 603–632, doi:10.1016/S0278-4343(01)00101-7.
- Tokuyay, T., G. Constantinescu, and J. Gonzalez-Castro (2009), Investigation of two elemental error sources in boat-mounted acoustic Doppler current profiler measurements by large eddy simulations, *J. Hydraul. Eng.*, 135(11), 875–887, doi:10.1061/(ASCE)HY.1943-7900.0000083.
- Vermeulen, B., A. J. F. Hoitink, and M. G. Sassi (2011), Coupled ADCPs can yield complete Reynolds stress tensor profiles in geophysical surface flows, *Geophys. Res. Lett.*, 38, L06406, doi:10.1029/2011GL046684.